Assessing Soil Sealing Dynamics in the Metropolitan Area of Bari Using Sentinel-2, Sealed Surface Index, and Machine Learning Approaches

Ahmad Asad[1,2], Alessandra Capolupo[2(✉)], and Eufemia Tarantino[2]

[1] Department of Agricultural and Environmental Sciences, University of Bari Aldo Moro, Bari, Italy
[2] Department of Civil, Environmental, Land, Construction and Chemistry (DICATECh), Politecnico di Bari, Via Orabona 4, 70125 Bari, Italy
alessandra.capolupo@poliba.it

Abstract. Soil sealing, the irreversible covering of natural soil with impermeable material, impacts environmental sustainability by degrading ecosystems and reducing water quality and infiltration capacity. Advanced geospatial detecting and monitoring approaches are, thus, needed to face this critical environmental challenge. This study assesses the effectiveness of two advanced geomatics approaches in detecting the dynamics of sealed surfaces in the metropolitan area of Bari from 2018 to 2024 using Sentinel-2 satellite imageries processed in Google Earth Engine: the sealed surface index and the machine learning-based Classification and Regression Trees algorithm. Twenty-eight Sentinel-2 imageries, acquired during February, May, July, and October, were analyzed. When necessary, a cloud cover masking process was employed before classification. After that, the filtered maps were classified with the two above-mentioned techniques generating four land cover classes: sealed surfaces, vegetation, bare land, and water bodies. Their accuracy was assessed against the training data gathered from the land use map provided by ISPRA. The outcomes demonstrated that incorporating machine learning significantly improved classification accuracy. The sealed surface class exhibited the highest classification accuracy, with Producer's and User's Accuracy consistently exceeding 90% and 85%, respectively. Conversely, bare soil proved more challenging to classify, leading to slightly lower accuracy values. These findings highlight the annual variations in sealed surfaces and their correlation with seasonal land-use dynamics. A notable increase in urban sealing, exceeding 2%, was observed between February 2018 and October 2024. This study underscores the importance of continuous monitoring of soil sealing for sustainable urban planning and environmental management.

Keywords: Soil Sealing · SUI · CART algorithm · Sustainability · Urbanization

© The Author(s), under exclusive license to Springer Nature Switzerland AG 2026
O. Gervasi et al. (Eds.): ICCSA 2025 Workshops, LNCS 15891, pp. 238–255, 2026.
https://doi.org/10.1007/978-3-031-97617-9_16

1 Introduction

Soil is a finite, essential, and crucial nonrenewable resource that has been abruptly covered with impermeable materials and excessive agricultural activities. This has led to the degradation of natural habitats and ecosystems, as well as a decline in water quality and infiltration capacity [1–3]. Such a phenomenon, commonly named "soil sealing", has been particularly evident in coastal areas worldwide over the past century [4, 5]. This is partly due to the historical oversight of urban planners regarding the environmental consequences of infrastructure expansion and the removal of soil cover, resulting in significant habitat loss [6].

Given its environmental impact, soil sealing analysis and monitoring have become a top priority of the European Union [7], resulting in the development of various methods to track and monitor Land Use/Land Cover (LU/LC) changes [8]. Advances in technology have significantly enhanced the observation of soil sealing patterns, with Remote Sensing (RS) emerging as a key tool in this field [9]. Indeed, it continuously provides multiscale information, offering, with time, a vital resource of global geospatial information without the need for direct field studies [10, 11]. However, RS has limitations, including the effects of weather conditions, particularly cloud cover and dust particles, that can distort imagery [12, 13] as well as limitations in spatial and temporal resolution [14]. In contrast, Remotely Piloted Aircraft Systems Services (RPAS) provide high-resolution, fine-scaled data making them particularly useful for local analysis [15, 16]. However, they are less suitable for large-scale studies due to the increased time and resources required for comprehensive data collection [17, 18].

Among the various satellite initiatives providing free open-source imagery, the Landsat mission, launched in 1972 by NASA/USGS, is the longest-running program [19]. Although it is particularly useful for long-term monitoring, its spatial resolution (30 m) is too coarse to detect LU/LC changes accurately. Thus, more recently, the Sentinel initiative, launched by the European Space Agency (ESA) in 2014, offers higher spatial resolution imagery (10 m) [20]. Nevertheless, both programs are widely used by researchers due to their accessibility and superior spatial resolution compared to the Moderate Resolution Imaging Spectroradiometer (MODIS) satellite, which has provided coarse resolution imagery of 250 m, 500 m, and 1 km at 36 spectral bands since 1999 [21]. Additionally, both Landsat and Sentinel imageries are adopted to extract LU/LC categories [22–25].

These LU/LC categories can be extracted using various approaches. Traditional pixel-based classification methods analyze individual entities based on spectral characteristics but fail to account for spatial relationships between neighboring pixels, limiting their effectiveness in higher-resolution datasets [26]. Nevertheless, among them, the index-based approach is suitable for quickly classifying the largest areas. Thus, proper indices were designed to monitor and detect impervious surfaces [27–30] but without considering the sealing of soil by agricultural activities, except the Sealed Urban Index (SUI), developed for Sentinel 2 satellite characteristics [31].

Object-Based Image Analysis (OBIA), on the other hand, is particularly suited for high-resolution imagery, as it differentiates shapes, sizes, and textures of spatial objects, making it ideal for heterogeneous and complex landscapes [32, 33]. However, OBIA requires significant computational power and processing time, especially for the larger

study areas [34], and it is not suited to handle coarse resolution satellite images [35]. Machine Learning (ML) algorithms, like Classification and Regression Tree (CART), offer an alternative approach by leveraging statistical and computational models to reduce classification errors and inconsistencies in LU/LC data. These algorithms excel in processing both medium and high-resolution imagery, and handling non-linear, large, and complex datasets [36]. However, their primary drawback is the need for extensive training and careful calibration of threshold parameters to achieve optimal results [37].

The primary aim of this study is to analyze the dynamics of soil sealing in the Bari metropolitan area, within the Puglia region, using advanced methodologies to detect, quantify, and monitor LU/LC based on Sentinel-2 satellite data over a period of about 6 years (2018–2024). To meet such a purpose, a temporal trend of soil sealing was analyzed for specific months (February, May, July, and October) to identify seasonal and long-term changes. Both pixel-based and machine learning techniques were employed, using the SU index and CART classifier to detect soil sealing and other LU/LC categories such as vegetation, bare soil, and water.

2 Materials and Methods

For this research, proper Sentinel 2 satellite images covering the metropolitan area of Bari were selected and handled within the Google Earth Engine (GEE) environment using a custom-developed JavaScript code. Before employing two different classification approaches, index-based and ML, a cloud masking procedure was applied, when necessary. The accuracy of the resulting maps was assessed by computing the confusion matrix, based on training data collected from the LU/LC map provided by Istituto Superiore per la Protezione e la Ricerca Ambientale (ISPRA). The entire process is summarized in the workflow reported in Fig. 1, while each step is detailed in the following subparagraphs.

2.1 Geodatabase and Pre-processing

The Sentinel satellite Level-2A (surface reflectance) dataset was picked up to achieve the research goal. The Level 2A product was first introduced on March 26, 2018, as the initial baseline and was subsequently refined based on quality control reports embedded in the product. Sentinel 2A is equipped with a MultiSpectral Instrument (MSI) that captures data across 13 bands at 10 m, 20 m, and 60 m spatial resolution. Specifically, four bands (Red (R), Green (G), Blue (B), Near-InfraRed (NIR)) operate at 10m resolution; six bands, including four narrow bands in Visible Near Infra-Red (VNIR) for vegetation red-edge spectral domain and two wider bands in Shortwave Infra-Red (SWIR), work at 20m resolution; and, the remaining three bands (Coastal Aerosol, Water Vapor, and SWIR-Cirrus), dedicated to atmospheric and aerosol monitoring, operate at 60m.

The ESA provides temporal offset values between bands [38] to ensure data consistency and minimize information loss. A significant offset can reduce the suitability of certain bands for direct combination in indices without mathematical corrections. Table 1 reports these values, highlighting that Bands 9 and 2 have an offset of 2.59s,

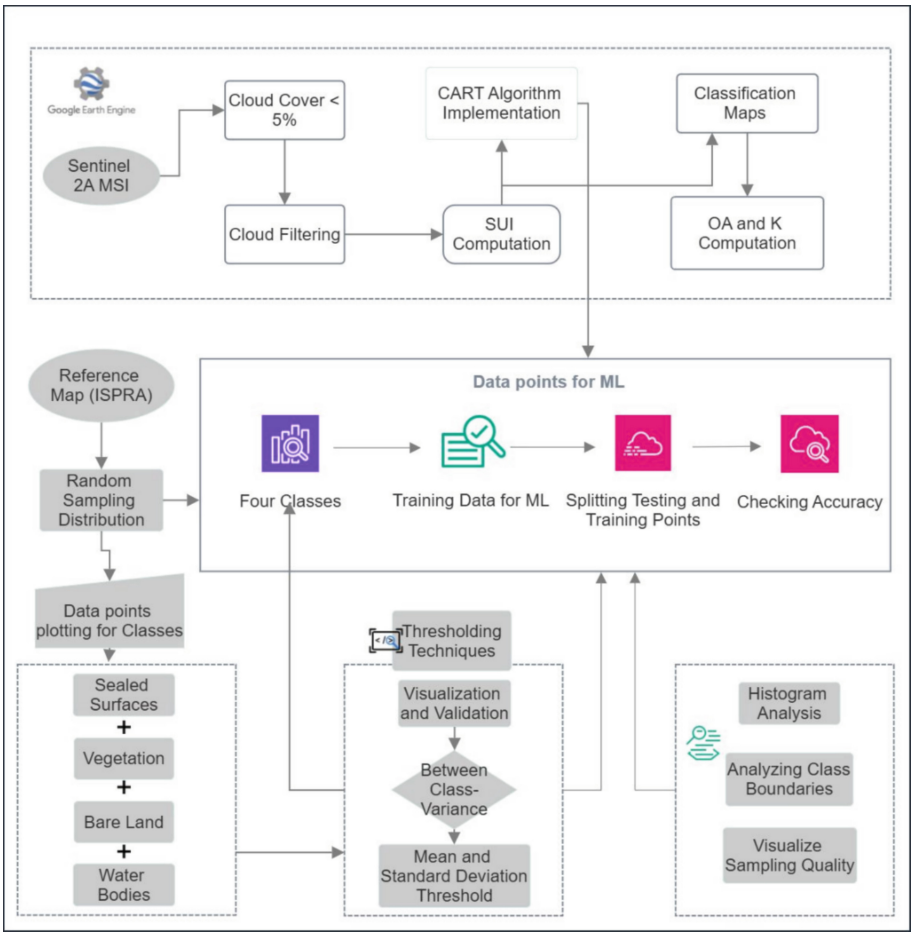

Fig. 1. Research workflow.

making them unsuitable for direct use together without appropriate adjustments. This parameter is crucial for identifying the optimal indices to extract LU/LC information.

As a result, Sentinel 2A images were selected as input data for this study. Specifically, 28 images, covering four different months (February, May, June, and October) from 2018 up to 2024, were gathered and processed in the GEE environment (https://earthengine.google.com/). These months were chosen to analyze seasonal trends in urban sprawl over the years, helping to minimize misclassifications caused by seasonal variations. Additionally, a cloud cover threshold (5%) was set to reduce clouds and shadow effects, ensuring high-quality data. The only exception was the May 2019 image, which exhibited a cloud cover of 18.34% due to generally high cloud cover in the Bari region during that month. Further details of the collected data are provided in Table 2.

Table 1. Wavelengths and temporal offset between bands in Sentinel 2.

Band Pair	Temporal Offset (s)	Band 1 Wavelength (nm)	Band 2 Wavelength (nm)
B08 / B02	0.264	842	490
B03 / B08	0.264	560	842
B03 / B02	0.527	560	490
B10 / B03	0.324	1375	560
B10 / B02	0.851	1375	490
B04 / B10	0.154	665	1375
B04 / B02	1.005	665	490
B05 / B04	0.264	705	665
B05 / B02	1.269	705	490
B11 / B05	0.199	1610	705
B11 / B02	1.468	1610	490
B06 / B11	0.057	740	1610
B06 / B02	1.525	740	490
B07 / B06	0.265	783	740
B07 / B02	1.790	783	490
B8a / B07	0.265	865	783
B8a / B02	2.055	865	490
B12 / B8a	0.030	2190	865
B12 / B02	2.085	2190	490
B01 / B12	0.229	443	2190
B01 / B02	2.314	443	490
B09 / B01	0.271	945	443
B09 / B02	2.586	945	490

Before starting the processing phase, the data were atmospherically corrected, and the clouds were masked using the approach proposed by [39]. However, geometric correction was not performed, as the data provided by USGS was already deemed satisfactory.

2.2 Processing Steps

Two approaches were adopted to extract LU/LC classes: a pixel-based analysis relying on the computation of the SUI and a ML-based approach utilizing the CART algorithm. Both methods are described in detail in the following sub-sections.

Table 2. Sentinel 2A image details.

Image IDs	Acquisition Date	Cloud Cover (%)
20180204T094159_20180204T094518_T33TXF	04/02/2018	3.36
20180525T094029_20180525T094824_T33TXF	25/05/2018	0.49
20180714T094029_20180714T094337_T33TXF	14/07/2018	0.23
20181012T094029_20181012T094403_T33TXF	12/10/2018	1.79
20190219T094039_20190219T094304_T33TXF	19/02/2019	0
20190505T094041_20190505T094230_T33TXF	05/05/2019	18.34
20190724T094041_20190724T094126_T33TXF	24/07/2019	0
20191012T094031_20191012T094345_T33TXF	12/10/2019	0.18
20200209T094131_20200209T094333_T33TXF	09/02/2020	0.04
20200207T095059_20200207T095055_T33TXF	07/02/2020	3.55
20200504T094029_20200504T094809_T33TXF	04/05/2020	0.44
20200701T095031_20200701T095501_T33TXF	01/07/2020	1.02
20201001T094039_20201001T094320_T33TXF	01/10/2020	2
20210203T094211_20210203T094345_T33TXF	03/02/2021	0
20210509T094029_20210509T094028_T33TXF	09/05/2021	0
20210701T095029_20210701T095030_T33TXF	01/07/2021	0
20211004T095031_20211004T095403_T33TXF	04/10/2021	0.01
20220203T094109_20220203T094111_T33TXF	03/02/2022	0.19
20220512T095031_20220512T095033_T33TXF	12/05/2022	4.06
20220703T094039_20220703T094036_T33TXF	03/07/2022	0
20221004T095029_20221004T095027_T33TXF	04/10/2022	0
20230201T095129_20230201T095130_T33TXF	01/02/2023	1.23
20230507T095031_20230507T095028_T33TXF	07/05/2023	0
20230703T094041_20230703T094035_T33TXF	03/07/2023	1.18
20231001T094031_20231001T094348_T33TXF	01/10/2023	4.19
20240203T094119_20240203T094116_T33TXF	03/02/2024	3.61
20240501T095031_20240501T095031_T33TXF	01/05/2024	3.92
20240705T094549_20240705T094718_T33TXF	05/07/2024	0.014
20241013T095029_20241013T095746_T33TXF	13/10/2024	0

Sealed Urban Index

Traditional pixel-based methods rely on the principle that different materials exhibit unique spectral reflectance signatures due to variations in the absorption and reflection of electromagnetic radiation. This approach enables the rapid classification of large areas. However, most existing indices were developed using Landsat data, making them

less suitable for Sentinel imagery. Additionally, many of these indices focus primarily on urban areas, limiting their applicability to broader land cover classifications. On the other hand, the SUI, specifically designed for Sentinel images, not only detects impervious surfaces (asphalt, concrete, buildings, roads) but also identifies overused agricultural land, where water infiltration is significantly reduced. SUI is calculated using Eq. 1:

$$SUI = \frac{(Green - SWIR1) \times (SWIR2 - Red)}{(Green + SWIR1) \times (SWIR2 + Red)} + 0.5. \quad (1)$$

However, as reported in a previous study [31], SUI alone does not yield highly accurate results. When combined with ML techniques, its efficiency improves significantly. Moreover, the integration of ML not only enhances the detection of sealed surfaces but also facilitates the identification of other land cover types, enabling a more effective differentiation among classes.

Classification Using the CART Algorithm

CART is a decision tree ML algorithm used for both classification and regression tasks [40]. It works by recursively partitioning the dataset into smaller, more homogeneous subsets. In this study, the CART model was employed to classify soil sealing and other LU/LC categories, dividing them into four distinct classes: sealed surfaces, vegetation, bare land, and water bodies. This partitioning process improved the accuracy of the model by making the classification more precise for the trained data. Indeed, training data are crucial for ML models, as inaccurate training can lead to misclassification and unreliable results. In this study, the training data were sourced from the ISPRA LU/LC map [41].

To remove the overlapping of the four data classes, the Otsu thresholding techniques were applied. Otsu's method, which minimizes intra-class variance, helped improve the separability between classes. Additionally, standard deviation (σ) and mean (μ) values were used for adaptive image thresholding. These techniques effectively removed redundancies and ensured clearer results in the testing phase.

To evaluate the performance of the model, the truth data collected on the ISPRA maps were split into 70% training data and 30% testing data. This split was performed automatically by the CART algorithm, and the final accuracy was calculated using the testing data. Because of the diverse LU/LC features, a random sampling distribution method was selected for the data points.

2.3 Accuracy Assessment

To evaluate the performance of the two applied approaches, a testing dataset was selected from the ISPRA map applying the random sampling techniques, used as ground truth. These points served as the input data for computing the confusion matrix and extracting the following statistical metrics: Overall Accuracy (OA), Producer accuracy (PA), User accuracy (UA), and Kappa coefficient (K). OA was used to check whether the pixels classified into the four different LU/LC classes were correctly assigned, while K was calculated to evaluate the reliability of the classification, as it accounts for chance agreements [42]. PA and UA were measured to determine whether classification results for each category fell within the acceptable accuracy thresholds [43].

2.4 Case Study of Bari

The study focuses on the Metropolitan City of Bari and its surrounding areas located in the Puglia region (Southern Italy) (Fig. 2). It is over 116 square kilometers, and it was selected as a pilot case since it was characterized by a significant urban and agricultural expansion over the last few decades. Indeed, Bari has experienced the most extensive urban sprawl in the entire Puglia region.

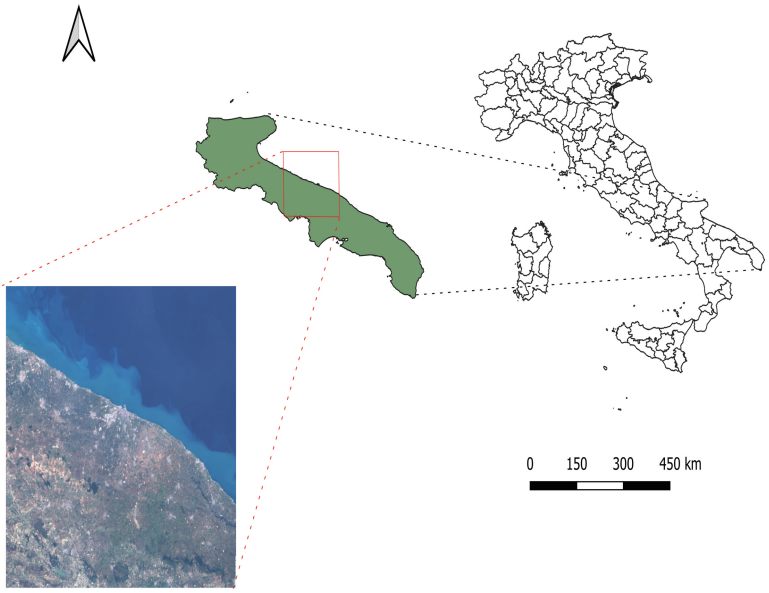

Fig. 2. Study area of Bari.

The urban sprawl along the Adriatic Sea coast of Bari city is one of the causes of the rapid expansion since the 21st century. Therefore, it was selected as pilot site.

3 Results and Discussion

This paper evaluates the effectiveness of the SU index for detecting sealed surfaces, both as a standalone method and when integrated with ML techniques. Its performance was tested over about six years, spanning from 2018 up to 2024, using a total of 28 images collected by Sentinel 2A.

The spatial distribution map of SUI results is depicted in Fig. 3, which presents a composite panel of classification maps corresponding to the selected months and years. Figure 3, a), b), c), d) represents 2018 images of February, May, July, and October respectively, while e), f), g), h) are February, May, July, and October of 2019 and so on.

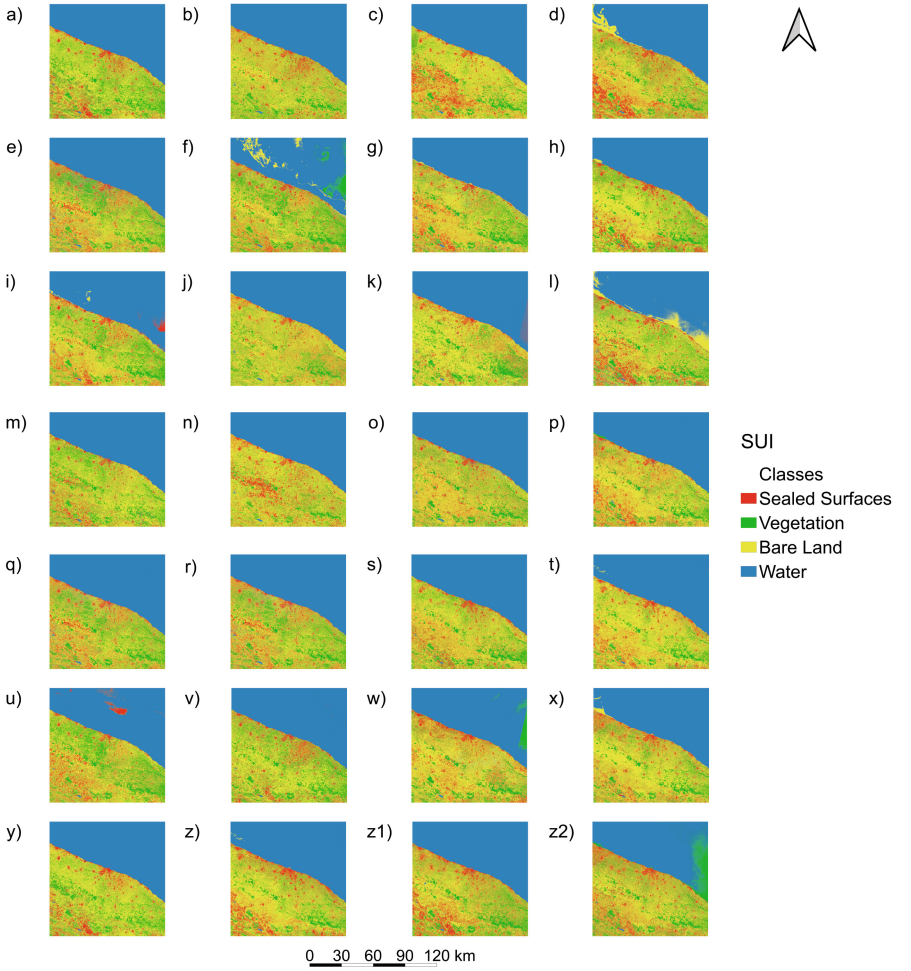

Fig. 3. Spatial representation of SUI.

Nonetheless, substantial cloud cover in the May 2019 image significantly affected outputs quality, as observed in Fig. 3 (f). This finding is also confirmed by the accuracy metrics reported at the end of this section. The analysis of the spatial LU/LC distribution around the metropolitan area of Bari indicates that SUI successfully detected overused agricultural lands, with and without the implementation of the ML algorithm. However, Fig. 4, which compares SUI results obtained with and without ML, suggests that incorporating ML enhances class differentiation.

The left panel (a) of Fig. 4, representing SUI outcome, primarily identifies impervious surfaces and a limited extent of overused agricultural land based on an image from February 2022. In contrast, the right panel (b) of Fig. 4, incorporating ML, clearly identifies all sealed surfaces, including overused agricultural land, with only minor misclassification of bare soil. Sealed surfaces are represented in red, frequently appearing

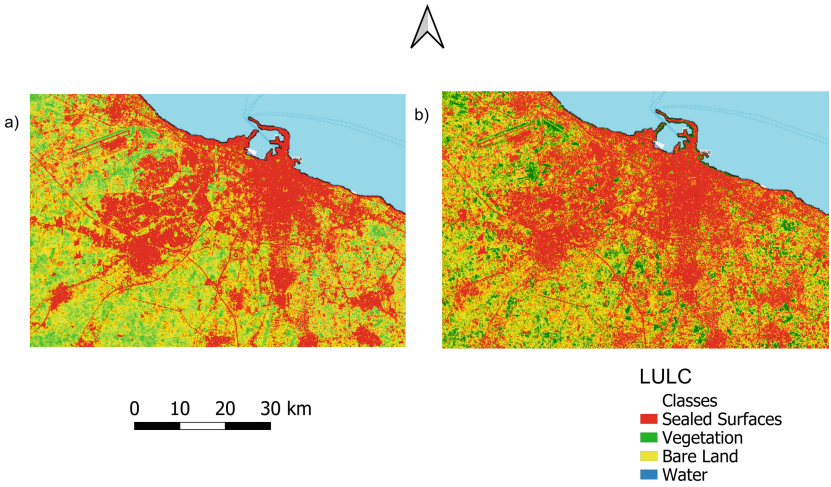

Fig. 4. Spatial representation of SUI (left) and ML outcomes (right).

along the coastal zone across all selected months and years. Seasonal variations were also observed, with sealed surfaces being more prevalent in the elevated areas opposite Bari and the Adriatic Sea during February and October, regions characterized by extensive agricultural activities.

An interesting finding pertains to the classification results of 2020, where a significant increase in the detection of abundant vegetation was observed. This trend is likely associated with the COVID-19 lockdown period, during which reduced human activities such as traffic and urbanization contributed to the enhancement of vegetation growth. Despite the persistence of urban sprawl, these findings suggest that decreased anthropogenic pressure may have positive ecological effects. The other three classes are vegetation, bare land, and water, which are represented in green, yellow, and blue, respectively. Bare soil has been slightly misclassified, as it was one of the most difficult classes to identify.

Table 3 depicts the OA and K for each image analyzed after applying ML. The results indicate consistently high classification accuracy, with OA exceeding 90% in most cases. K values greater than 0.81 indicate that the results from the supervised classification produced reliable results. However, the image collected in May 2019 exhibited lower accuracy ($< 90\%$) and a K value of 0.8008 due to excessive cloud cover, which introduced distortions into the classification process. In contrast, the metrics generated by using the SU index standalone showed slightly lower OA and K values (Table 4). Nevertheless, although OA is lower than 90%, K values remain above 0.80, suggesting that even SUI still produces promising results. The May 2019 image also yielded the lowest results for SUI, with a K value of 0.7826, again due to cloud cover.

Simultaneously, Tables 4 and 5 describe the PA and UA generated from the CART algorithm and SUI, respectively. The former shows that PA and UA consistently exceeded 90% and 85%, respectively, across all images. In contrast, the bare land class exhibited the lowest accuracy, with PA and UA values mostly falling below 90%, while the vegetation

Table 3. Kappa coefficient (K) and Overall Accuracy (OA) of the CART algorithm.

Image IDs	K	OA (%)
20180204T094159_20180204T094518_T33TXF	0.86	91
20180525T094029_20180525T094824_T33TXF	0.86	91
20180714T094029_20180714T094337_T33TXF	0.89	93
20181012T094029_20181012T094403_T33TXF	0.86	92
20190219T094039_20190219T094304_T33TXF	0.86	92
20190505T094041_20190505T094230_T33TXF	0.80	88
20190724T094041_20190724T094126_T33TXF	0.86	92
20191012T094031_20191012T094345_T33TXF	0.90	93
20200209T094131_20200209T094333_T33TXF	0.86	91
20200207T095059_20200207T095055_T33TXF	0.86	91
20200504T094029_20200504T094809_T33TXF	0.85	92
20200701T095031_20200701T095501_T33TXF	0.94	97
20201001T094039_20201001T094320_T33TXF	0.91	94
20210203T094211_20210203T094345_T33TXF	0.89	93
20210509T094029_20210509T094028_T33TXF	0.90	94
20210701T095029_20210701T095030_T33TXF	0.86	92
20211004T095031_20211004T095403_T33TXF	0.86	94
20220203T094109_20220203T094111_T33TXF	0.88	93
20220512T095031_20220512T095033_T33TXF	0.92	95
20220703T094039_20220703T094036_T33TXF	0.85	90
20221004T095029_20221004T095027_T33TXF	0.85	90
20230201T095129_20230201T095130_T33TXF	0.89	93
20230507T095031_20230507T095028_T33TXF	0.91	94
20230703T094041_20230703T094035_T33TXF	0.90	93
20231001T094031_20231001T094348_T33TXF	0.92	95
20240203T094119_20240203T094116_T33TXF	0.89	92
20240501T095031_20240501T095031_T33TXF	0.86	92
20240705T094549_20240705T094718_T33TXF	0.89	93
20241013T095029_20241013T095746_T33TXF	0.86	91

class maintained excellent accuracy, surpassing 90%. It is noteworthy that the sealed surface class achieved higher PA and UA values in most winter images, whereas bare land tended to perform worse during the summer months. As shown in Table 3, images captured in July over the years yielded excellent results, with OA above 90% and K

Table 4. Kappa coefficient (K) and Overall Accuracy (OA) of SUI.

Image IDs	K	OA (%)
20180204T094159_20180204T094518_T33TXF	0.82	90
20180525T094029_20180525T094824_T33TXF	0.81	90
20180714T094029_20180714T094337_T33TXF	0.84	91
20181012T094029_20181012T094403_T33TXF	0.83	90
20190219T094039_20190219T094304_T33TXF	0.83	91
20190505T094041_20190505T094230_T33TXF	0.78	86
20190724T094041_20190724T094126_T33TXF	0.82	90
20191012T094031_20191012T094345_T33TXF	0.84	92
20200209T094131_20200209T094333_T33TXF	0.81	80
20200207T095059_20200207T095055_T33TXF	0.82	90
20200504T094029_20200504T094809_T33TXF	0.81	90
20200701T095031_20200701T095501_T33TXF	0.85	93
20201001T094039_20201001T094320_T33TXF	0.83	91
20210203T094211_20210203T094345_T33TXF	0.83	91
20210509T094029_20210509T094028_T33TXF	0.84	91
20210701T095029_20210701T095030_T33TXF	0.83	90
20211004T095031_20211004T095403_T33TXF	0.81	91
20220203T094109_20220203T094111_T33TXF	0.82	91
20220512T095031_20220512T095033_T33TXF	0.85	92
20220703T094039_20220703T094036_T33TXF	0.81	90
20221004T095029_20221004T095027_T33TXF	0.80	89
20230201T095129_20230201T095130_T33TXF	0.82	91
20230507T095031_20230507T095028_T33TXF	0.83	91
20230703T094041_20230703T094035_T33TXF	0.85	93
20231001T094031_20231001T094348_T33TXF	0.83	91
20240203T094119_20240203T094116_T33TXF	0.83	91
20240501T095031_20240501T095031_T33TXF	0.82	90
20240705T094549_20240705T094718_T33TXF	0.85	92
20241013T095029_20241013T095746_T33TXF	0.83	91

values greater than 0.85. This is likely due to the favorable weather conditions in July, when minimal rainfall results in less distorted satellite imagery.

Tables 4 and 6, which present the results of SUI, show lower accuracy across all images compared to those processed with ML. Specifically, UA and PA values for all classes were somewhat reduced when ML was not employed, as detailed in Table 6.

Table 5. PA and UA obtained from CART algorithm.

Acquisition Date	PA - Sealed Surfaces	PA - Vegetation Class	PA - Bare Land	PA - Water	UA - Sealed Surfaces	UA - Vegetation Class	UA - Bare Land	UA - Water
02/04/18	85	94	89	100	92	95	80	100
05/25/18	90	94	83	100	95	96	76	100
07/14/18	89	94	94	100	97	98	80	100
10/12/18	88	98	79	100	91	92	88	80
02/19/19	99	77	88	100	97	100	73	75
05/05/19	95	86	80	75	88	92	81	75
07/24/19	91	91	84	100	85	97	84	100
10/12/19	98	98	74	100	96	97	85	100
02/09/20	86	93	89	100	92	93	81	100
05/09/20	97	94	74	100	91	95	77	100
07/23/20	93	92	86	100	93	90	83	100
10/21/20	92	98	98	100	98	98	88	100
02/03/21	98	92	96	100	95	99	83	100
05/09/21	93	98	81	100	89	94	93	100
07/23/21	96	97	86	100	96	100	87	100
10/21/21	92	91	87	100	89	94	90	100
02/03/22	98	88	88	67	97	97	97	67
05/14/22	95	90	88	100	90	98	88	100
07/23/22	96	99	85	100	90	98	91	100
10/16/22	87	94	88	100	90	90	87	100
02/18/23	91	91	84	100	89	96	79	100
05/29/23	94	90	83	100	90	96	86	100
07/18/23	90	97	89	100	90	90	92	100
10/11/23	90	93	87	100	97	93	83	100
02/08/24	98	93	97	75	93	99	88	100
05/23/24	90	96	90	100	93	98	83	100
07/17/24	88	91	80	100	89	95	78	100
10/15/24	94	90	88	100	94	98	79	100

Notably, even in the May 2019 image, despite a higher cloud cover percentage, the accuracy for sealed surfaces remained high, demonstrating the robustness of this index under challenging conditions.

Table 6. PA and UA generated from SUI.

Acquisition Date	PA - Sealed Surfaces	PA - Vegetation Class	PA - Bare Land	PA - Water	UA - Sealed Surfaces	UA - Vegetation Class	UA - Bare Land	UA - Water
02/04/18	84	92	88	100	90	92	77	100
05/25/18	90	94	80	100	93	94	73	100
07/14/18	88	93	92	100	96	98	78	100
10/12/18	87	98	78	100	90	91	86	80
02/19/19	98	75	86	100	96	100	71	75
05/05/19	90	86	78	75	87	90	78	75
07/24/19	89	90	81	100	84	96	82	100
10/12/19	97	97	72	100	94	96	82	100
02/09/20	83	92	87	100	91	93	79	100
05/09/20	96	93	73	100	90	94	76	100
07/23/20	92	91	84	100	93	89	81	100
10/21/20	91	97	96	100	97	97	85	100
02/03/21	97	91	94	100	95	97	82	100
05/09/21	91	97	79	100	89	93	91	100
07/23/21	95	95	85	100	95	99	85	100
10/21/21	91	90	80	100	88	94	88	100
02/03/22	96	86	86	70	96	96	95	70
05/14/22	94	88	87	100	89	95	87	100
07/23/22	95	97	83	100	89	96	90	100
10/16/22	85	92	86	100	90	90	86	100
02/18/23	91	90	84	100	88	96	78	100
05/29/23	94	89	81	100	89	94	83	100
07/18/23	89	95	87	100	89	88	91	100
10/11/23	89	92	86	100	97	92	82	100
02/08/24	91	93	90	75	91	96	85	100
05/23/24	90	95	88	100	90	97	81	100
07/17/24	87	91	78	100	88	94	76	100
10/15/24	93	89	86	100	91	97	78	100

4 Conclusion

This study assesses the performance of the SU index standalone and integrated into the CART algorithm for mapping sealed surfaces and detecting their changes over about 6 years (2018–2024). The two techniques were tested on 28 Sentinel 2A images collected

over the metropolitan area of Bari in order to analyze the sealed surface variations across seasons and years.

Study results highlight the effectiveness of SUI in detecting and mapping sealed surfaces, particularly when combined with machine learning techniques. Indeed, the integration of SUI with CART significantly enhances classification accuracy, facilitating a more precise differentiation of sealed surfaces with vegetation and bare land, as enhanced in the confusion matrix. Despite minor misclassifications, the high accuracy levels observed in this study underscore the reliability of SUI for large-scale land monitoring applications. However, the challenge of accurately classifying bare soil slightly reduced the OA. Despite this, the classification still achieved satisfying results, with OA consistently exceeding 90% for all tested images captured in February, May, July, and October from 2018 to 2024. The only exception was affected by a higher percentage of cloud cover, which significantly reduced accuracy.

These findings support the analysis of annual variations in sealed surfaces. In the metropolitan area of Bari, sealed surfaces increased by more than 2%. Specifically, the sealed surface class measured 10 m^2 in February 2018 and reached 15 m^2 in October 2024. SU index and the outcomes of this research will assist urban planners in developing more effective sustainable solutions, as the identification of different classes is crucial. Furthermore, this research will also provide insights into monitoring changes in different geospatial features, supporting urban planners and policymakers to develop new sustainable cities.

References

1. Fini, A., Frangi, P., Mori, J., Donzelli, D., Ferrini, F.: Nature based solutions to mitigate soil sealing in urban areas: Results from a 4-year study comparing permeable, porous, and impermeable pavements. Environ. Res. **156**, 443–454 (2017)
2. Capolupo, A., Barletta, C., Esposito, D., Tarantino, E.: Earth observation data for sustainable management of water resources to inform spatial planning strategies. In: Marucci, A., Zullo, F., Fiorini, L., Saganeiti, L. (eds.) Innovation in Urban and Regional Planning. INPUT 2023. Lecture Notes in Civil Engineering, vol. 467, pp. 24–35. Springer, Cham (2024). https://doi.org/10.1007/978-3-031-54118-6_3
3. Morabito, M., et al.: The impact of built-up surfaces on land surface temperatures in Italian urban areas. Sci. Total. Environ. **551–552**(1), 317–326 (2016)
4. Mannucci, S., Kwakkel, H., Morganti, M., Ferrero, M.: From past to future: understanding urban development in flood-prone coastal Rome. J. Urban Des., 1–32 (2024)
5. Smiraglia, D., Cavalli, A., Giuliani, C., Assennato, F.: The increasing coastal urbanization in the mediterranean environment: the state of the art in Italy. Land **12**(5), 1017 (2023)
6. Hamilton, B., Coops, C.N., Lokman, K.: Time series monitoring of impervious surfaces and runoff impacts in Metro Vancouver. Sci. Total. Environ. **760**(15), 143873 (2021)
7. Tombolini, I., Rodrigo-Comino, J., Salvati, L.: Toward a sustainable use of land: urbanization, policies and (mis)understanding of degradation processes. In: Land Quality and Sustainable Urban Forms. Springer Geography, pp. 17–74. Springer, Cham (2022). https://doi.org/10.1007/978-3-030-94732-3_2
8. Peroni, F., et al.: How to map soil sealing, land take and impervious surfaces? A systematic review. Environ. Res. Lett. **17**, 053005 (2022)

9. Säurich, A., Möller, M., Gerighausen, H.: A novel remote sensing-based approach to determine loss of agricultural soils due to soil sealing — a case study in Germany. Environ. Monit. Assess. **196**, 510 (2024)
10. Mastrorosa, S., Crespi, M., Congedo, L., Munafò, M.: Land consumption classification using sentinel 1 data: a systematic review. Land **12**, 932 (2023)
11. Barletta, C., Capolupo, A., Tarantino, E.: Copernicus geodatabase for investigating land cover changes at the European scale. In: Marucci, A., Zullo, F., Fiorini, L., Saganeiti, L. (eds.) Innovation in Urban and Regional Planning. INPUT 2023. Lecture Notes in Civil Engineering, vol. 467, pp. 12–23. Springer, Cham (2024). https://doi.org/10.1007/978-3-031-54118-6_2
12. Shen, H., Li, H., Qian, Y., Zhang, L., Yuan, Q.: An effective thin cloud removal procedure for visible remote sensing images. ISPRS J. Photogramm. Remote Sens. **96**, 224–235 (2014)
13. Lan, X., Zhang, L., Shen, H., Yuan, Q., Li, H.: Single image haze removal considering sensor blur and noise. EURASIP J. Adv. Sign. Proces., 1–13 (2013)
14. Wang, Q., Tang, Y., Ge, Y., Xie, H., Tong, X., Atkinson, M.P.: A comprehensive review of spatial-temporal-spectral information reconstruction techniques. Sci. Remote Sens. **8**, 100102 (2023)
15. Pour, T., Miřijovský, J., Purket, T.: Airborne thermal remote sensing: the case of the city of Olomouc, Czech Republic. Eur. J. Remote Sens. **52**(sup1), 209–218 (2019)
16. Pepe, M., Fregonese, L., Scaioni, M.: Planning airborne photogrammetry and remote-sensing missions with modern platforms and sensors. Eur. J. Remote Sens. **51**(1), 412–436 (2018)
17. Saponaro, M., Tarantino, E.: LULC classification performance of supervised and unsupervised algorithms on UAV-Orthomosaics. In: Gervasi, O., Murgante, B., Misra, S., Rocha, A.M.A.C., Garau, C. (eds.) Computational Science and Its Applications – ICCSA 2022 Workshops. ICCSA 2022. Lecture Notes in Computer Science, vol. 13379, pp. 311–326. Springer, Cham (2022). https://doi.org/10.1007/978-3-031-10545-6_22
18. Saponaro, M., Capolupo, A., Tarantino, E., Fratino, U.: Comparative analysis of different UAV-based photogrammetric processes to improve product accuracies. In: Misra, S., et al. Computational Science and Its Applications – ICCSA 2019. ICCSA 2019. Lecture Notes in Computer Science, vol. 11622, pp. 225–238. Springer, Cham (2019). https://doi.org/10.1007/978-3-030-24305-0_18
19. Landsat Missions. https://www.usgs.gov/landsat-missions. Accessed 2 Feb 2025
20. The Sentinel missions. https://www.esa.int/Applications/Observing_the_Earth/Copernicus/The_Sentinel_missions. Accessed 1 Feb 2025
21. MODIS. https://modis.gsfc.nasa.gov/about/index.php. Accessed 13 Feb 2025
22. Capolupo, A., Tarantino, E.: Landsat 9 satellite images potentiality in extracting land cover classes in GEE environment using an index-based approach: the case study of Savona City. In: Gervasi, O., et al. Computational Science and Its Applications – ICCSA 2023 Workshops. ICCSA 2023. Lecture Notes in Computer Science, vol. 14107, pp. 251–265. Springer, Cham (2023). https://doi.org/10.1007/978-3-031-37114-1_17
23. Capolupo, A., Monterisi, C., Saponaro, M., Tarantino, E.: Multi-temporal analysis of land cover changes using Landsat data through Google Earth Engine platform. In: Proceedings of the Eighth International Conference on Remote Sensing and Geoinformation of the Environment (RSCy2020), vol. 11524, pp. 447–458. SPIE (2020)
24. Aguilar, M.A., Jiménez-Lao, R., Ladisa, C., Aguilar, F.J., Tarantino, E.: Comparison of spectral indices extracted from Sentinel-2 images to map plastic covered greenhouses through an object-based approach. GIScience Remote Sens. **59**(1), 822–842 (2022)

25. Capolupo, A., Santoro, P.M., Tarantino, E.: Exploiting medium-resolution sentinel data in google earth engine for burned area reflectance classification. In: Gervasi, O., Murgante, B., Garau, C., Taniar, D., C. Rocha, A.M.A., Faginas Lago, M.N. (eds.) Computational Science and Its Applications – ICCSA 2024 Workshops. ICCSA 2024. Lecture Notes in Computer Science, vol. 14819, pp. 201–216. Springer, Cham (2024). https://doi.org/10.1007/978-3-031-65282-0_13
26. Misra, I., Rohil, M.K., Manthira Moorthi, S., Dhar, D.: Feature based remote sensing image registration techniques: a comprehensive and comparative review. Int. J. Remote Sens. **43**(12), 4477–4516 (2022)
27. Tian, Y., Chen, H., Song, Q., Zheng, K.: A novel index for impervious surface area mapping: development and validation. Remote Sensimh **10**, 1521 (2018)
28. Sun, G., Chen, X., Jia, X., Yao, Y., Wang, Z.: Combinational Build-up Index (CBI) for effective impervious surface mapping in urban areas. IEEE J. Sel. Top. Appl. Earth Observations Remote Sens. **9**(5), 2081–2092 (2016)
29. Bouhennache, R., Bouden, T., Taleb-Ahmed, A., Cheddad, A.: A new spectral index for the extraction of built-up land features from Landsat 8 satellite imagery. Geocartography Int. **34**(14), 1531–1551 (2019)
30. Zhang, L., Tian, Y., Liu, Q.: A novel urban composition index based on water-impervious surface-pervious surface (W-I-P) model for urban compositions mapping using landsat imagery. Remote Sens. **13**, 3 (2021)
31. Asad, A., Capolupo, A., Tarantino, E.: Machine learning and index-based classification approaches for accurately evaluating sealed surfaces from medium-resolution Sentinel 2 data. In: Proceedings of the 4th International Proceedings of Mediterranean Geosciences Union. Scopus, Barcelona (2025)
32. Sarzana, T., Maltese, A., Capolupo, A., Tarantino, E.: Post-processing of pixel and object-based land cover classifications of very high spatial resolution images. In: Gervasi, O., et al. Computational Science and Its Applications – ICCSA 2020. ICCSA 2020. Lecture Notes in Computer Science, vol. 12252, pp. 797–812. Springer, Cham (2020). https://doi.org/10.1007/978-3-030-58811-3_57
33. Blaschke, T.: Object based image analysis for remote sensing. ISPRS J. Photogramm. Remote Sens. **65**(1), 2–16 (2010)
34. Liu, D., Xia, F.: Assessing object-based classification: advantages and limitations. Remote Sens. Lett. **1**(4), 187–194 (2010)
35. Johnson, A.B., Ma, L.: Image segmentation and object-based image analysis for environmental monitoring: recent areas of interest, researchers' views on the future priorities. Remore Sens. **12**(11), 1772 (2020)
36. Waghela, H., Patel, S., Sudesan, P., Raorane, S., Borgalli, R.: Land use land cover classification using machine learning. In: Proceedings of the 2022 International Conference on Automation, Computing and Renewable Systems (ICACRS), Pudukkottai, India, pp. 708–711 (2022)
37. Milojevic-Dupont, N., Creutzig, F.: Machine learning for geographically differentiated climate change mitigation in urban areas. Sustain. Cities Soc. **64**, 102526 (2021)
38. Binet, R., Bergsma, E., Poulain, V.: Accurate Sentinel-2 inter-band time delays. ISPRS Annals of the Photogrammetry, Remote Sensing and Spatial Information Sciences, vol. V-1–2022 XXIV ISPRS Congress (2022 edition), Nice, France (2022)
39. Sola, I., et al.: Assessment of atmospheric correction methods for Sentinel-2 images in Mediterranean landscapes. Int. J. Appl. Earth Obs. Geoinf. **73**, 63–76 (2018)
40. Sarker, H.I.: Machine learning: algorithms, real-world applications and research directions. SN Comput. Sci. **2**, 160 (2021)

41. Geological and Geotematics Map. https://www.isprambiente.gov.it/en/databases/data-base-collection/soil-and-territory/geological-and-geotematics-map. Accessed 13 Jan 2025
42. Moody, M.G.: Explaining the unsuitability of the kappa coefficient in the assessment and comparison of the accuracy of thematic maps obtained by image classification. Remote Sens. Environ. **239**, 111630 (2020)
43. Nicolau, A.P., Dyson, K., Saah, D., Clinton, N.: Accuracy assessment: quantifying classification quality. In: Cardille, J.A., Crowley, M.A., Saah, D., Clinton, N.E. (eds.) Cloud-Based Remote Sensing with Google Earth Engine, pp. 135–145. Springer, Cham (2024). https://doi.org/10.1007/978-3-031-26588-4_7